Quantitative phase imaging by common-path interferometric microscopy: application to super-resolved imaging and nanophotonics

Vicente Micó,[a] Javier García,[a] and Zeev Zalevsky[b]

[a]Dep. de Óptica, Universitat de València, C/ Dr. Moliner 50, 46100 Burjassot, Spain
vicente.mico@uv.es, javier.garcia.monreal@uv.es
[b]School of Engineering, Bar-Ilan University, Ramat-Gan 52900, Israel
zalevsz@eng.biu.ac.il

Abstract. Quantitative phase imaging needs of a holographic setup in order to retrieve the sample phase distribution. Often this new phase information is obtained at the cost of reducing the useful range in other parameters of the imaging system such as field of view or resolution. We devised an experimental setup that allows complex amplitude evaluation and phase image quantification of three-dimensional (3-D) samples in wide-field digital holographic microscopy. The basis is a common-path interferometric configuration that can be implemented in two configurations depending on the position and the basic period of the grating: static grating and windowed Fourier filtering method or with phase-shifting moving grating. Both configurations allow complex amplitude recovery and, thus, quantitative phase imaging of the sample under test. Moreover, by combining the basic setup with tilted illumination and time multiplexing, it is possible to generate a synthetic aperture enlargement that improves the final image resolution. Experimental results validated our concepts.

Keywords: digital holographic microscopy, quantitative phase imaging, common-path interferometry, time multiplexing superresolution, synthetic aperture generation.

1 INTRODUCTION

Digital holography is a powerful tool that allows fast, non-contact, full-field, high-resolution quantitative complex amplitude measurements of objects [1,2]. The amplitude distribution of the imaging beam is added in the hologram plane with a reference wave and the hologram is recorded by using a CCD camera. Then, the object wavefront is reconstructed numerically [3-6] by simulating the back propagation of the complex amplitude using the Kirchhoff-Fresnel propagation equations.

During the recent past, digital holography has been combined with microscopy to avoid the limited depth of focus in high numerical aperture (NA) lenses and the high magnification ratios needed in conventional optical microscope imaging. The basic architecture is defined by a interferometric configuration where the imaging system is placed on one branch (imaging arm) and a reference beam is reinserted at the CCD plane incoming from the second branch (reference arm). Due to its interferometric underlying principle, different classical interferometric configurations can be employed. Thus, we find Mach–Zehnder [7], Michelson [8], Twyman–Green [9], and common-path [10] interferometers as basis architectures in digital holographic microscopy.

In particular, common-path interferometers are especially interesting because of the robustness and simplicity of the system, which is more stable, relatively insensitive to vibrations and require fewer optical elements than other interferometric configurations previously presented in the literature. In a common-path interferometric setup, both the imaging and the reference for the interferometric recording follow nearly the same optical path. Thus the instabilities of the system (mechanical or due to thermal changes on both optical paths) do not affect the obtained results. Common-path interferometers had been proposed in many different forms such as the point-diffraction [11], dark-ground filtering

Received 14 Jan 2009; accepted 20 May 2009; published 29 May 2009 [CCC: 19342608/2009/$25.00]

[12], phase-contrast [13,14] and luminance contrast method [15], and are applied to visualization of phase disturbances [16-19], quantitative phase imaging [20-22], wavefront and phase aberration sensing [23,24], and superresolution imaging [25-27].

In this paper, we report on a common-path interferometric architecture that is applied to microscopy. It is based on the input plane spatial multiplexing and the addition of a diffraction grating at the image space. Firstly, the spatial multiplexing means that the input plane is composed from the sample under test in side-by-side configuration with a blank region. In this configuration, part of the illumination beam passes the input plane without being distorted by the input sample and can be used as reference beam in the interferometric recording process. Secondly, the addition of a diffraction grating at the image space allows the mixing of both beams and hence the interference. But such grating can be placed in two different configurations (see Fig. 1): just at the Fourier plane of the imaging lens or moved away from this plane. Thus, we have distinguished two different cases that are related with the position of the grating. Notice that, in both cases, the digital recording device (a CCD camera) is placed at the position of the output plane where the input sample is directly imaged (zero order of the grating) by the imaging system (see Fig. 1).

On one hand and when the grating is placed just at the Fourier plane of the objective lens, an on-axis image plane hologram is recorded by the CCD. This former case is characterized by the absence of a bias carrier frequency between both interferometric beams and the grating must be phase-shifted in order to recover the complex amplitude field of the imaged sample. On the other hand, when the grating is placed far enough from the Fourier plane and assuming that the basic period of the grating and its position are well matched, an off-axis image plane hologram is recorded. This fact is due to the reference beam reaches the CCD forming an angle with the propagation direction of the imaging beam. In this latter case, as well as by applying phase-shifting method, it is possible to recover the complex transmitted field by considering the following process: Fourier transforming the recorded hologram, filtering and centering the spectral distribution located at one of the hologram diffraction orders, and coming back to the spatial domain by another Fourier transformation operation.

Obviously, there are a lot of situations where the grating can be placed between the two previously commented cases. In those cases, the diffraction orders of the recorded hologram will overlap with the zero order term because the bias carrier frequency is not high enough to avoid the overlapping. For those situations, the only way to retrieve the complex amplitude distribution is by using phase-shifting procedure.

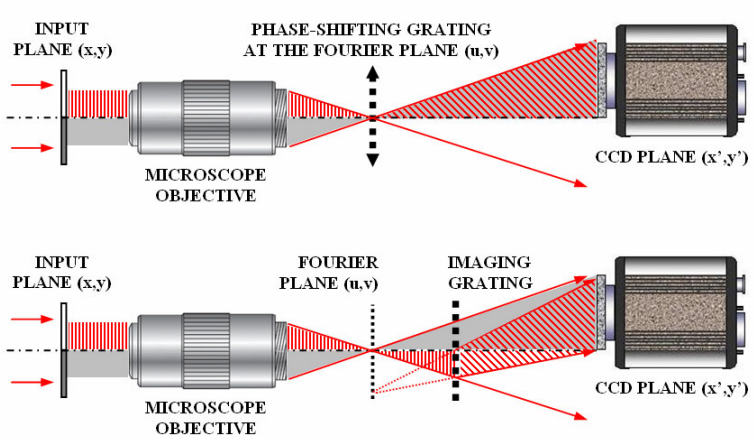

Fig. 1. Conceptual difference between on-axis (up) and off-axis (down) holographic recording cases. We can see the graphical definition of the bias carrier frequency for the off-axis case.

In addition, by placing another diffraction grating in the blank region and by using tilted illumination onto the input plane, it is possible to assure the transmission of a

reference beam through the imaging lens. That reference beam is originated in one of the diffraction orders of such grating: in that one that diffract on-axis of the impinging tiled beam according with the illumination angle, the illumination wavelength and the basic grating period. But tilted illumination is also responsible for the on-axis diffraction of additional spatial-frequency content of the input sample that is not accessible under conventional on-axis illumination. In this case, different spatial-frequency bands of the sample spectrum can be recovered in time sequence and can be properly managed to generate a synthetic aperture that expands up the frequency space coverage of the microscope objective, or in other words, it allows superresolved imaging of the sample.

An important last note is related to the connection of the proposed techniques to nano photonics. The relation to nano photonics is made in two senses. First, the components added to the proposed configurations include gratings which may contain spatial features below 400 nm (e.g. multi level diffraction grating). Second, the proposed approaches allow obtaining 3-D profile and phase distribution at nano metric resolution and steps. Furthermore, the proposed methods allow generation of lateral two-dimensional (2-D) super resolved imaging which once again can approach resolution limits allowing separation spatial of features below 400 nm when dealing with the visible light spectrum.

Along this paper, we will review in Sec. 2 the mathematic theory of the two proposed common-path interferometric setups while Sec. 3 will present experimental results where quantitative phase and superresolved imaging is achieved in both proposed configurations. Finally, Sec. 4 will conclude the paper.

2 THEORETICAL ANALYSIS

In this section we review the mathematical foundations of the basic setup corresponding with a common-path interferometric imaging approach. Although the theoretically analyzed setup is composed from a 4F optical processor in order to gain in simplicity, the proposed analysis is completely useful for the case when using a microscope objective by taking into account its magnification. The following scheme is proposed: we first derive the equation describing the input plane amplitude distribution and later we separately analyze the two proposed cases: on-axis recording with phase-shifting technique and off-axis recording with windowed Fourier filtering method.

The basic optical setup is depicted in Fig. 2. A collimated on-axis beam illuminates the input plane incoming from a point source placed at the axial point of the focal plane of a collimation lens. Although at this moment we are only interested in on-axis illumination, we will derive the formalism considering the possibility of a tilted beam represented by a carrier frequency of $(\nu_n, \nu_m) = (\sin\theta_n/\lambda, \sin\theta_m/\lambda)$ incoming from a generic off-axis source originated at a point of coordinates (x_n, y_m) of the source plane and a 2-D reference grating in side-by-side configuration with the input sample. This procedure will make easier the mathematical analysis of the superresolution section. Thus, Eq. (1) provides the amplitude distribution at the input plane after being illuminated with a monochromatic plane-wave having a generic bias carrier frequency of (ν_n, ν_m)

$$U_{IP}(x,y)=\left[t(x,y)+\sum_{n,m} C_n C_m \exp\left\{-j2\pi\nu_0 (nx+my)\right\}\right] A\exp\left\{-j2\pi\left[\nu_n x+\nu_m y\right]\right\}, \qquad (1)$$

where $t(x,y)=\left|t(x,y)\right| exp\left(i\phi_0(x,y)\right)$ is the sample complex amplitude function defined from $\left|t(x,y)\right|$ and $\phi_0(x,y)$ as its real amplitude and phase distributions respectively. Also note that (x, y) are the spatial coordinates, λ is the illumination wavelength, (n, m) are the diffraction orders of the 2-D generalized reference grating, (C_n, C_m) and v_0 are the amplitude coefficients and the basic frequency of the 2-D reference grating in both X and Y directions respectively, and A is the amplitude of the illumination beam originated at the position defined by (x_n, y_m).

2.1 On-axis recording case.

Now, we focus on the case when the imaging grating is placed just at the Fourier plane of the imaging system. In this configuration, the first lens in Figure 2 performs Fourier transformation of the input plane amplitude distribution onto its focal image plane, where a one-dimensional (1-D) imaging grating is placed. Then, the amplitude distribution at the system Fourier plane equals

$$U_{FP}(u,v)=FT\{U_{IP}(x,y)\}\ \mathrm{circ}\left(\frac{\rho}{\Delta v}\right)\sum_{p}B_p\exp\{j2\pi pv'u\}, \tag{2}$$

with *(u,v)* the spatial-frequency coordinates, ρ the polar coordinate in the frequency domain that is defined as $\rho=\sqrt{u^2+v^2}$, *circ* the function that represents the limited system aperture with a width of Δv, and (B_P, v') the amplitude coefficient and the basic frequency of the imaging grating, respectively.

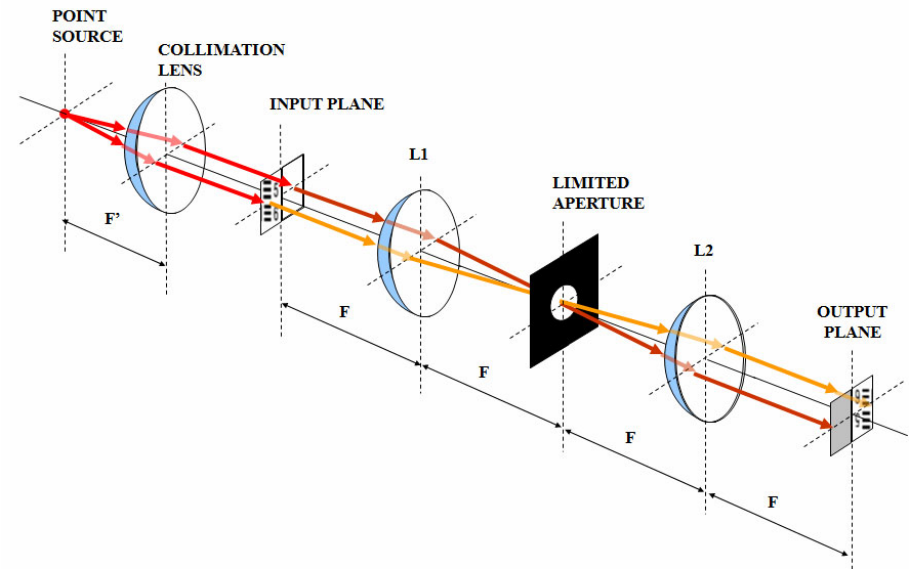

Fig. 2. Basic geometry for theoretical analysis of a common-path interferometric imaging approach.

After that, the second lens performs a second Fourier transformation between Fourier and output planes. Leaving aside constant factors, the final amplitude distribution provided by the imaging system at the system output plane is proportional to

$$U_{OP}(x',y')=U_{IP}(-x',-y')\otimes \mathrm{disk}(\Delta v\ r)\otimes\sum_{p}\delta(x'-p\lambda Fv'), \tag{3}$$

where *disk(Δv r)* is the point spread function (PSF) of the 4F processor, *r* is the polar coordinate that is defined as $r=\sqrt{x'^2+y'^2}$, and λF the scale factor of the second Fourier transformation.

Paying attention to Eq. (3), the last convolution comes from the imaging grating and it means that the transmitted band-pass image is replicated at the output plane. Considering on-axis illumination for simplicity, that is, $(x_n, y_m) = (0,0)$, Eq. (3) can be rewritten as

$$U_{OP}^{\text{on-axis}}(x',y')=\left[\left(t(-x',-y')+C_0\right)\otimes\sum_p\delta\left(x'-p\lambda Fv'\right)\right]\otimes \text{disk}\left(\Delta v\ r\right), \tag{4}$$

Between square brackets, we can see that the input plane amplitude distribution is replicated at the output plane according with the basic frequency of the imaging grating. Thus, by properly selecting the basic period of the imaging grating, it is possible to overlap at the output plane the imaging beam (incoming from the input sample) and the reference beam (incoming from the blank region or from a given diffraction order of the reference grating at the input plane). So, on-axis holographic recording will be produced.

In order to recover both amplitude and phase distributions of the transmitted frequency band-pass, a phase-shifting method is applied. Due to the CCD is placed at the position of the output plane where the input sample is directly imaged, the hologram is composed from the zero and -1 diffraction orders of the imaging grating that is responsible for the imaging and the reference beams, respectively. In that sense, the phase of the reference beam can be modulated in time by shifting the imaging grating, which means a phase modulation of the recorded hologram and allows phase-shifting strategy.

Conceptually, the CCD camera is limiting the field of view of the image because it selects only the field of view position where the sample image is formed. So, the intensity distribution recorded at the CCD at a given instant *t* and due to a generic point source originated at (x_n, y_m) position comes from the addition of the imaging beam (sample band-pass image selected by such source convolved with the PSF of the imaging system) and an on-axis reference beam due to the imaging grating

$$I_{OP}(x',y',t)=\left|\left(t(-x',-y')\,A\,e^{-j2\pi\left[\nu_n x'+\nu_m y'\right]}\right)\otimes \text{disk}\left(\Delta v\ r\right)+C\,e^{j\left[\phi_S(x',y')+\phi_m(t)\right]}\right|^2, \tag{5}$$

with C a constant related to the real amplitude of the reference beam, ϕ_S the initial phase difference between imaging and reference beams which is directly related with the transmitted phase distribution of the sample band-pass due to the source placed at (x_n, y_m), and ϕ_m the linear phase increment introduced in time between two subsequent intensity images. Note that linear phase variation in time is assumed. Assuming that the time dependence of the recorded intensity can be expressed as a function of the intensity image number m multiplied by the phase step between two consecutive images ($\phi_m = m\phi_k$) and taken the different intensity distributions in time sequence, Eq. (5) can be rewritten as

$$\begin{aligned} I_{OP}^{m}(x',y',t_m)=&\left|\left(t(-x',-y')\,\exp\left\{j2\pi\left[\nu_n x'+\nu_m y'\right]\right\}\right)\otimes \text{disk}\left(\Delta v\ r\right)\right|^2+C^2 \\ &+2C\,\text{Re}\left[\left(t(-x',-y')\,\exp\left\{j2\pi\left[\nu_n x'+\nu_m y'\right]\right\}\right)\otimes \text{disk}\left(\Delta v\ r\right)\right]\cos\left(\phi_S+m\phi_k\right) \end{aligned}, \tag{6}$$

Then, by using phase-shift algorithm and computing the different I_m intensity distributions stored by the CCD, it is possible to recover each transmitted phase distribution $\phi_S(x', y')$ of the input object due to each (x_n, y_m) illumination source. In particular, we have applied a method (see Ref. 2) that takes into account p intensity images in one phase-shift period and permits the recovering of the initial phase distribution according to

$$\phi_S(x',y')=\text{Arg}\left\{\sum_{m=1}^{p} I_m(x',y')\exp\left[-j\frac{2\pi}{p}(m-1)\right]\right\}, \tag{7}$$

This procedure allows us to recover the phase distribution, and therefore the object complex amplitude, of each one of the frequency bands transmitted through the system aperture when illumination incoming from the position (x_n, y_m) in the source plane is

considered. Notice that each source position (x_n, y_m) selects a different spatial-frequency content of the sample spectrum by the linear phase factor that multiplies the sample amplitude distribution; see Eq. (6). In that sense, by properly adjusting the off-axis positions (x_n, y_m) of the point sources with the radius ($\Delta\nu$) of the system aperture, a contiguous band-pass content of the sample spectrum will be diffracted on-axis and will be recovered by applying phase-shifting method.

For validating the proposed setup as a common-path phase-shifting microscopy configuration only on-axis illumination provided by the axial point source $(x_n, y_m) = (0,0)$ is considered. However, for the superresolution implementation, different off-axis source positions must be lighted on in sequential mode and every frequency band-pass is sequentially recovered. After that and by properly placing them on its original position, a wider spectral content of the object can be fully reconstructed in terms of synthetic aperture generation. Thus, provided that there will be a diffraction order in the reference grating for each off-axis source position, any synthetic aperture can be shaped.

2.2 Off-axis recording case.

Coming back to the amplitude distribution of the Fourier plane but without adding the imaging grating, we see that the second lens of the 4F optical processor performs another Fourier transformation and the following amplitude distribution is generated at the output plane

$$U_{OP}(x',y') = \left[U_{IP}(-x',-y') A \exp\left\{ j2\pi \left[\nu_n x' + \nu_m y' \right] \right\} \right] \otimes \mathrm{disk}(\Delta\nu\, r), \tag{8}$$

But now, the 1-D imaging grating is placed between the second lens *L2* and the output plane (see Fig. 3) or between the Fourier plane of the microscope lens and the output plane (see Fig. 1). In any case, the imaging grating provides replicas of the output plane having a lateral shift that depends on the ν' (the basic frequency of the imaging grating) and the distance between the imaging grating and the output plane. As seen in Fig. 3, three replicas incoming from the three diffraction orders of the grating are considered. Once again, the CCD is placed at the position where the direct sample image is formed. This fact is marked by an enhanced black rectangle at the output plane in Fig. 3 where we can see as an off-axis reference beam will also reach this position. So, the intensity recorded at the CCD becomes

$$I_{CCD}(x',y') = \left| \left[t(-x',-y') A \exp\left\{ j2\pi \left[\nu_n x' + \nu_m y' \right] \right\} \right] \otimes \mathrm{disk}(\Delta\nu\, r) + B_1 \exp\left\{ j2\pi\nu' x' \right\} \right|^2, \tag{9}$$

Equation (9) results in 4 terms when square modulus is expanded. Once the intensity distribution is stored in the computer memory, we perform digitally an inverse Fourier transformation. Centered at the origin, we have the PSF of the imaging system coming from the tilted reference beam and the autocorrelation of the transmitted sample frequency band-pass due to the source position (x_n, y_m) that has a total width of $4\Delta\nu$. And moved from the origin, we find the two diffraction holograms orders representative of the complex and conjugate amplitude distribution of the transmitted sample frequency band-pass.

If the basic period of the imaging grating is properly selected, that is, the imaging grating must have a basic frequency larger than half the size of the zero order term ($2\Delta\nu$) plus half the size of the system frequency band pass (circular aperture with a width of $\Delta\nu$), then the diffraction orders will not overlap with the central term and the transmitted band can be recovered by filtering in the Fourier domain. To allow this windowed Fourier filtering process we need that $\nu' \geq 3\Delta\nu$. Equation (10) represents one of such hologram diffraction orders where we can see as the source position (x_n, y_m) selects the transmitted sample frequency content through the limited system aperture which is convolved with a delta function provided by the reference beam that is diffracted at the imaging grating

$$FT\{I_{CCD}(x',y')\}=...+\left[\tilde{t}(u+v_n,v+v_m)\,\mathrm{circ}\left(\frac{\rho}{\Delta v}\right)\right]\otimes\delta(u+v',v)+..., \qquad (10)$$

Then, by sequential process in time, every frequency band pass transmitted through the circular aperture and due to each (x_n, y_m) source it can be recovered and properly placed to its original position in the sample spectrum in such a way that a wider sample spectrum can be fully reconstructed in terms of the definition of a synthetic aperture.

As in the previous case, only the axial point source $(x_n, y_m) = (0,0)$ will be considered for validating the proposed setup as a common-path phase-shifting microscopy configuration but different off-axis source positions will be taken into account sequentially for superresolution purposes.

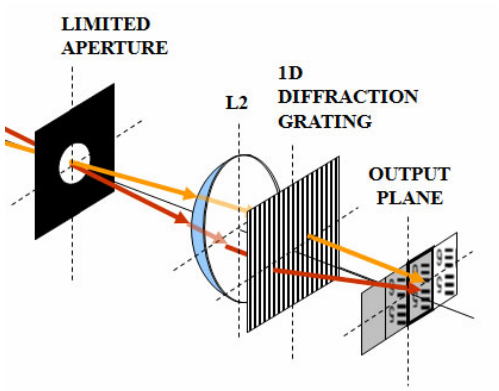

Fig. 3. Inclusion of the imaging grating in the setup depicted in Fig. 1.

3 EXPERIMENTAL RESULTS

In this section we present experimental results corresponding with quantitative phase imaging and superresolution validation for both previously studied configurations. Different experimental setups have been assembled at the laboratory considering different optical elements showing the easiness implementation and use of both proposed configurations.

3.1 On-axis recording case

First, we start with the case of on-axis recording and phase-shifting procedure. For this part, we have selected a 0.14NA Mitutoyo objective as imaging lens and a swine sperm bio-sample enclosed in a counting chamber as input object. The sperm cells have a head dimension of 6x9 μm corresponding with the height and width of the ellipsoidal shape of the head, a total length of 55 μm, and a tail width of 2 μm on the head side and below 1 μm on the end, approximately.

Light coming from a laser diode can (λ = 650 nm, 7 mW optical power) is used as point divergent illumination in the experimental setup. The diode module is placed onto a 2-D linear motion stage to allow tilted illumination over the input plane by shifting its position in sequential mode.

As it was previously stated, the input plane is composed by the swine sperm bio-sample and a 1-D Ronchi ruling grating with a basic period of 2.5 μm (400 lp/mm) playing the role of reference grating. This fact means that the reference grating diffracts the incoming beam at an angle of 15.1 degrees corresponding with its first diffraction order for the used illumination light. Or in other words, a reference beam will be diffracted on-axis by the action of the first grating order when a 15.1 degrees tilted beam impinges onto the reference grating.

But when a 15.1 degrees tilted beam illuminates the input sample, a quasi-contiguous frequency band is diffracted on-axis through the system aperture because the angle defined by the NA of the microscope lens is 8 degrees (that is, near the half angle of the off-axis illumination). Thus, it is possible to cover the full 2-D frequency space of the input plane by sequential exposures where the 2-D tilted illumination is properly matched with the diffraction orientation of the reference grating. To allow this, the reference grating is rotated according with the incidence direction of the off-axis illumination. So, a resolution gain factor close to 3 will be achieved in every frequency space direction.

A CCD camera (Kappa DC2, 12bits, 1352x1014 pixels with 6.7 μm pixel size) is used as imaging device while a 1-D Ronchi ruling grating (80 lp/mm) that is placed on a motorized linear translation stage is used as imaging grating. Then, a displacement on the grating of 12.5 μm implies a complete phase cycle in the recorded hologram.

The phase-shifting procedure is applied to each single source position in time sequence in such a way that the phase shift is produced by a linear shift of the imaging grating equal to 0.5 μm. As the period of the imaging grating is 12.5 μm, 25 consecutive images compose a whole phase cycle. As result, 8 off-axis frequency bands plus one addition on-axis band are recovered after apply phase-shifting procedure and are assembled into a single synthetic aperture by replacing the different off-axis frequency bands to its original position of the bio-sample spectrum. Figure 4 depicts the generated synthetic aperture composed by 9 elementary apertures in comparison with the conventional aperture.

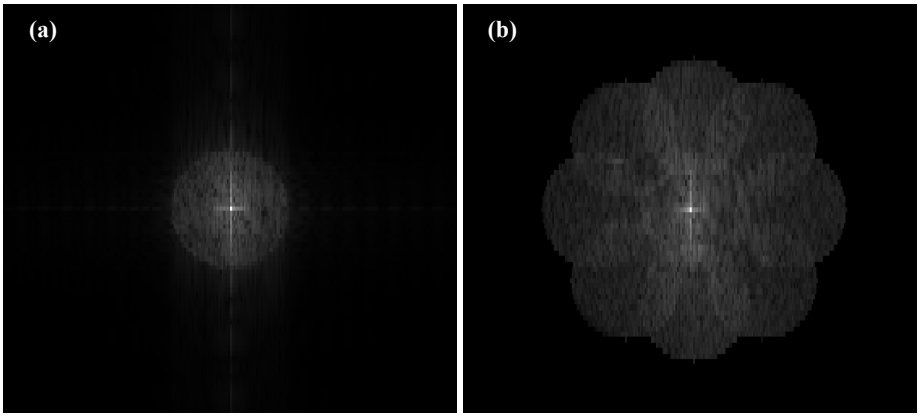

Fig. 4. (a) Conventional aperture obtained with on-axis illumination and (b) expanded synthetic aperture after applying the proposed approach.

Finally, a high-quality superresolved image is obtained by Fourier transformation of the information contained in the generated synthetic aperture. Figure 5 shows the superresolved image obtained by using the proposed approach in comparison with the low-resolution one produced when only on-axis illumination is considered.

Theoretically, the Rayleigh resolution limit of the 0.14NA lens is around 7 μm for the 650 nm wavelength of the illumination light. According with the size of the swine sperm cells, this value is in the limit of imaging the swine sperm head [Fig. 5 (a)]. When implementing the proposed approach, the value of the generated synthetic NA (SNA) can be numerically calculated as $SNA = NA_{source}+NA_{objective} \cong 0.4$. This fact means that the theoretical resolution limit of the synthetic imaging system is 2 μm approximately according with the Rayleigh criterion. That is, it enables image formation of the heads of the cells while the tails become to be resolved in its wider side (head side) and non resolved in the thinner side (ending tail side) as we can see in Fig. 5(b).

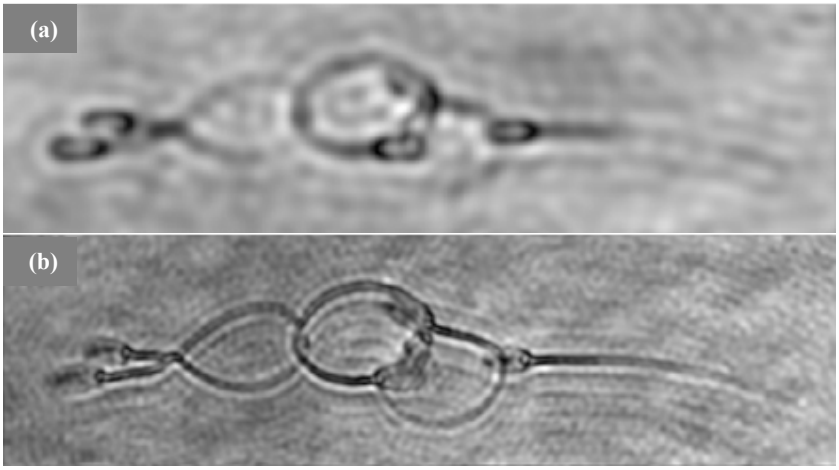

Fig. 5. Group of swine sperm cells: (a) conventional image considering on-axis illumination and (b) superresolved image provided by the proposed approach.

Figure 6 depicts the 3-D representations corresponding with the unwrapped phase distribution of both images presented in Fig. 5. We can see as, because of the fact that the complex amplitude distribution becomes superresolved, by plotting in 3-D the superresolved phase information we can achieve superresolved quantitative phase imaging [Fig. 6(b)].

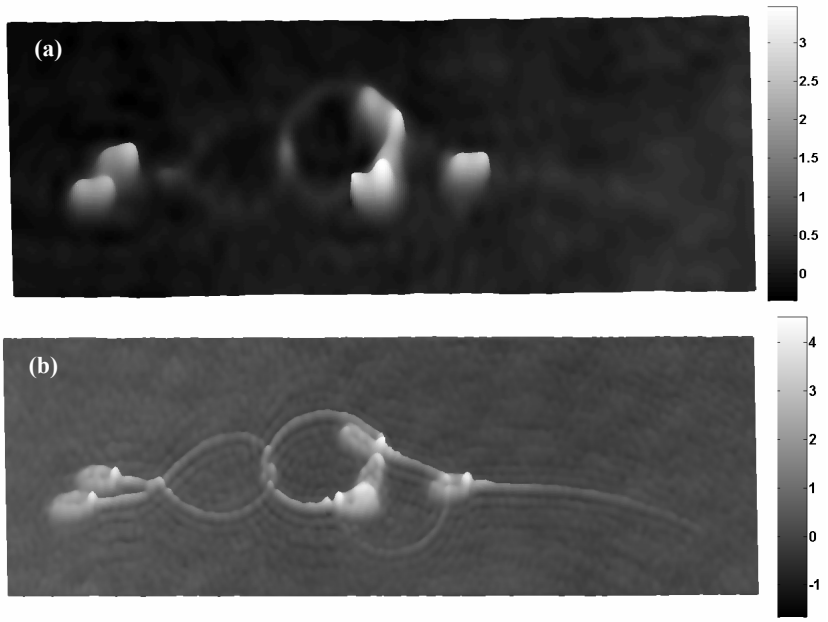

Fig. 6. Group of swine sperm cells: 3-D representations of the unwrapped phase distribution for (a) conventional on-axis illumination imaging mode corresponding with Fig. 5(a), and (b) superresolved imaging corresponding with Fig. 5(b). Gray scale represents optical phase in radians.

3.2 Off-axis recording case

In this second experimental section, we show the case of off-axis recording and windowed Fourier filtering method. For the superresolution validation, we have selected a cross shape of 3x3 VCSEL sources of a 2-D array that are sequentially lighted on. Those VCSEL sources are monochromatic with $\lambda = 850$ nm and have a beam divergence of ±15 deg. As imaging system we propose a Nikon microscope objective with 0.1NA that is used to image a positive USAF resolution test target. The imaging grating has a

period of 80 lp/mm and it is placed appropriately in front of the CCD to perform suitable holographic recording.

Attached to the object, we place a 2-D holographic grating with a period of 5 μm. Thus, when a 10 deg tilted collimated beam of 850 nm wavelength impinges on the input plane, the first diffraction order of the reference grating goes on axis. Once again, since this angle is near to be double of the one being defined by the NA of the microscope objectives, a resolution gain factor close to 3 will be achieved. In order to obtain a tilted collimated beam, the VCSEL array is placed in the object focal plane of a collimation lens (80 mm focal length). Thus, sequential activation of the VCSELs will provide the different tilts in the incoming illumination. Figure 7 depicts the recorded holograms for the case when three VCSEL sources in cross shape are considered and their respective Fourier transformations. Thus, cases (a)-(b), (c)-(d), and (e)-(f) correspond with the on-axis, horizontal off-axis and vertical off-axis illumination sources respectively. We can see as the transmitted frequency band-passes are moved far away from the central term avoiding overlapping and can be recovered by filtering and centring process.

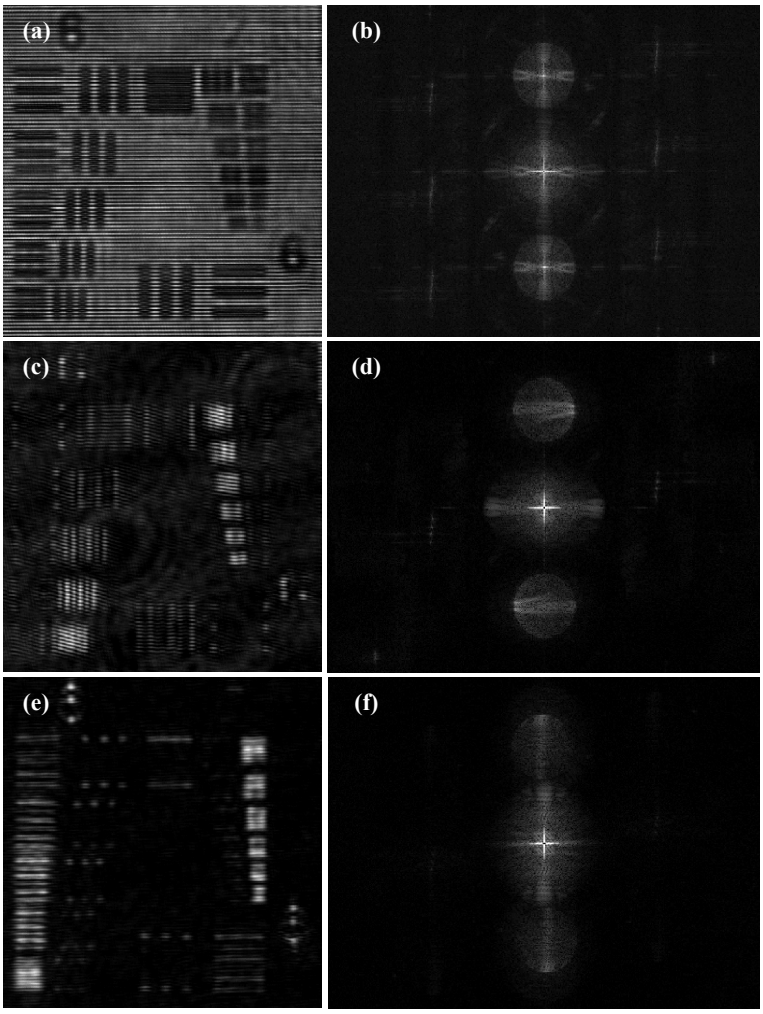

Fig. 7. Recorded holograms and their Fourier transformations for the Nikon lens: (a)-(b) on-axis illumination, (c)-(d) off-axis horizontal illumination, and (e)-(f) off-axis vertical illumination

Finally, Fig. 8 depicts the synthetic aperture enlargement and the superresolved image obtained by Fourier transformation of the information contained in the synthetic aperture in comparison with the conventional image when on-axis illumination is considered.

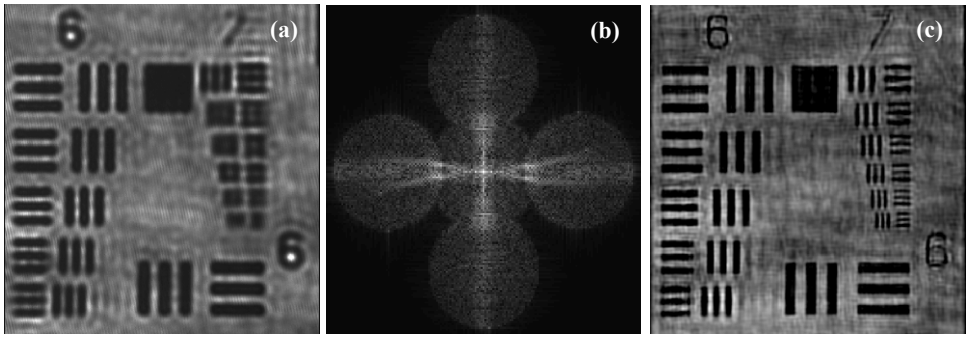

Fig. 8. Comparison between (a) conventional on-axis illumination and (c) superresolved images, and the cross-shape synthetic aperture (b) generated in the proposed experiment.

Common-path interferometric microscopy in off-axis recording mode has also been applied to the case of the bio-sample described in the previous section. But now, we have tried to achieve a higher SNA value when perform the proposed approach. As illumination source we use a He-Ne laser (λ = 632.8 nm) and as imaging lens we use the 0.42NA Mitutoyo objective. Off-axis illumination is achieved by using a diffraction grating to illuminate the input plane. Since the illumination grating has a period of 0.83 μm, it diffracts the incoming beam at an angle of 49.7 degrees corresponding with its first diffraction order. Once again, as the tilted illumination angle is doubling the angle defined by the NA of the microscope lens (24.8 deg), the generated synthetic aperture presents a cutoff frequency 3 times higher than the conventional one.

According to the theoretical definition provided by the Rayleigh criterion, the microscope lens has a resolution spot size of 1.84 μm which is not enough to image the tail's narrower part of the sperm cells [Fig. 9(a)]. After applying the proposed approach, the resolution spot size is reduced until 0.64 μm (corresponding with the theoretically achieved SNA value) and the whole sperm cell is resolved [Fig. 9(b)]. This fact means a resolution gain factor close to 3. Figure 9 is representative of such improvement in resolution while Fig. 10 depicts the 3-D plot of the unwrapped phase distribution allowing quantitative superresolved phase imaging of the swine sperm cells.

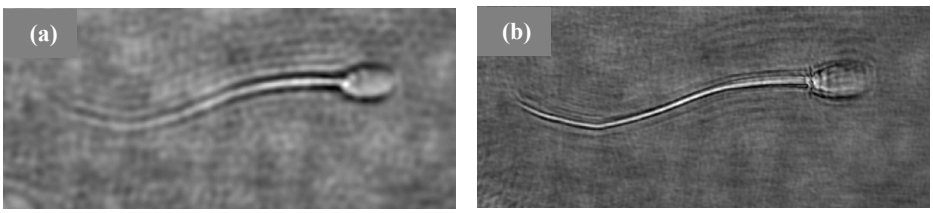

Fig. 9. Comparison between (a) conventional on-axis illumination and (b) superresolved images.

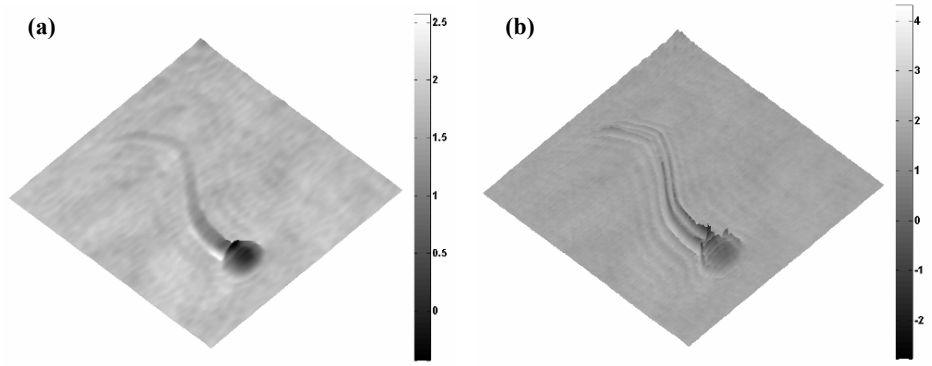

Fig. 10. 3-D plots of the unwrapped phase distributions for (a) conventional on-axis illumination imaging mode and (b) superresolved imaging. Grey level bars represent optical phase in radians.

4 CONCLUSIONS

We have proposed two different experimental setups based on a common-path interferometric architecture that allow superresolved and quantitative phase imaging of 3-D samples in wide-field digital holographic microscopy. In the first one, on-axis holographic recording is achieved by placing the imaging grating near the Fourier plane of the imaging lens. Thus, phase-shifting procedure is needed to recover the complex amplitude distribution transmitted through the imaging lens. In the second one, off-axis holographic recording is produced by placing the imaging grating far from the Fourier plane. In this case, windowed Fourier filtering is applied to recover the transmitted complex amplitude distribution. Both configurations have been tested considering synthetic (USAF resolution test) and phase (bio-sample) objects.

As strong point, the proposed configurations have a minimum of optical elements in the experimental setup since both are based on a common-path interferometric architecture. Thus, the imaging and the reference beams follow nearly the same optical path providing to the experimental setup three main advantages. First, the instabilities of the system, due to mechanical or thermal changes on both optical paths, do not affect the obtained results. Second, low coherence length light sources are suitable to be used as illumination. Third, the experimental setup becomes easy-to-configure and it is useful for implementation in microscopes having low and medium NA lenses where only simple modifications are required.

Additionally, tilted illumination can be performed using a single VCSEL element which is moved to off-axis positions or a 2-D VCSEL array with fixed single sources. This VCSEL array allows recording of each frequency band-pass in a short time due to its high optical power per every emitter and allows the possibility to perform spatial filtering by simple modulating the relative intensity of the different VCSEL elements. This fact allows synthetic aperture shaping if also the reference grating is properly selected depending on the aimed aperture.

References

[1] U. Schnars and W. P. Jueptner, *Digital Holography*, Springer, Heidelberg, Germany (2005) [doi:10.1007/b138284].

[2] T. Kreis, *Handbook of Holographic Interferometry: Optical and Digital Methods*, Wiley, New York (2005).

[3] W. S. Haddad, D. Cullen, J. C. Solem, J. W. Longworth, A. McPherson, K. Boyer, and C. K. Rhodes, "Fourier-transform holographic microscope," *Appl. Opt*. **31**, 4973-4978 (1992) [doi:10.1364/AO.31.004973].

[4] U. Schnars and W. P. O. Jüptner, "Direct recording of holograms by a CCD target and numerical reconstruction," *Appl. Opt*. **33**, 179-181 (1994) [doi:10.1364/AO.33.000179].

[5] S. Grilli, P. Ferraro, S. De Incola, A. Finizio, G. Pierattini, and R. Meucci, "Whole optical wavefields reconstruction by digital holography," *Opt. Exp*. **9**, 294-302 (2001).

[6] L. P. Yaroslavsky, *Digital Holography and Digital Image Processing: Principles, Methods*, *Algorithms*, Kluwer, Dordrecht, The Netherlands (2003).

[7] F. Charrière, J. Kühn, T. Colomb, F. Montfort, E. Cuche, Y. Emery, K. Weible, P. Marquet, and C. Depeursinge, "Characterization of microlenses by digital holographic microscopy," *Appl. Opt*. **45**, 829-835 (2006) [doi:10.1364/AO.45.000829].

[8] H. Iwai, C. Fang-Yen, G. Popescu, A. Wax, K. Badizadegan, R. R. Dasari, and M. S. Feld, "Quantitative phase imaging using actively stabilized phase-shifting low-coherence interferometry," *Opt. Lett*. **29**, 2399-2401 (2004) [doi:10.1364/OL.29.002399].

[9] S. Reichelt and H. Zappe, "Combined Twyman-Green and Mach-Zehnder interferometer for microlens testing," *Appl. Opt*. **44**, 5786-5792 (2005) [doi:10.1364/AO.44.005786].

[10] J. Glückstad and P. C. Mogensen, "Optimal phase contrast in common-path interferometry," *Appl. Opt*. **40**, 268-282 (2001) [doi:10.1364/AO.40.000268].
[11] R. N. Smart and W. H. Steel, "Theory and application of point diffraction interferometers," *Jpn. J. Appl. Phys*. **14**, 351-356 (1975).
[12] R. Carpentier and R. Champeau, "A simple though rigorous method for dealing with spatial filtering problems," *Eur. J. Phys*. **24** 543-552 (2003) [doi:10.1088/0143-0807/24/5/311].
[13] F. Zernike, "How I discovered phase contrast," *Science* **121**, 345-349 (1955) [doi:10.1126/science.121.3141.345].
[14] J. Glückstad, "Phase contrast image synthesis," *Opt. Comm*. **130**, 225-230 (1996) [doi:10.1016/0030-4018(96)00339-2].
[15] J. Piper, "Luminance-contrast – a new visible light technique for examining transparent specimens," *Micros. Today* **15(**4), 26-34 (2007).
[16] H. Kadono, N. Takai, and T. Asakura, "New common-path phase-shifting interferometer using a polarization technique," *Appl. Opt*. **26**, 898-904 (1987) [doi:10.1364/AO.26.000898].
[17] C. S. Anderson, "Fringe visibility, irradiance, and accuracy in common path interferometers for visualization of phase disturbances," *Appl. Opt.* **34**, 7474-7485 (1995) [doi:10.1364/AO.34.007474].
[18] V. Arrizón and D. Sánchez-de-la-Llave, "Common-path interferometry with one dimensional periodic filters," *Opt. Lett.* **29**, 141-143 (2004) [doi:10.1364/OL.29.000141].
[19] C. Meneses-Fabian, G. Rodriguez-Zurita, J. F. Vazquez-Castillo, C. Robledo-Sanchez, and V. Arrizón, "Common-path phase-shifting interferometer with binary grating," *Opt. Comm.* **264**, 13-17 (2006) [doi:10.1016/j.optcom.2006.02.024].
[20] G. Popescu, L. P. Deflores, J. C. Vaughan, K. Badizadegan, H. Iwai, R. R. Dasari, and M. S. Feld, "Fourier phase microscopy for investigation of biological structures and dynamics," *Opt. Lett*. **29**, 2503-2505 (2004) [doi:10.1364/OL.29.002503].
[21] G. Popescu, T. Ikeda, R. R. Dasari, and M. S. Feld, "Diffraction phase microscopy for quantifying cell structure and dynamics," *Opt. Lett*. **31**, 775-777 (2006) [doi:10.1364/OL.31.000775].
[22] G. Rodriguez-Zurita, C. Meneses-Fabian, N. Toto-Arellano, J. F. Vázquez-Castillo, and C. Robledo-Sánchez, "One-shot phase-shifting phase-grating interferometry with modulation of polarization: case of four interferograms," *Opt. Exp*. **16**, 7806-7817 (2008) [doi:10.1364/OE.16.007806].
[23] H. Medecki, E. Tejnil, K. A. Goldberg, and J. Bokor, "Phase-shifting point diffraction interferometer," *Opt. Lett*. **21**, 1526-1528 (1996) [doi:10.1364/OL.21.001526].
[24] H. Elfström, A. Lehmuskero, T. Saastamoinen, M. Kuittinen, and P. Vahimaa, "Common-path interferometer with a diffractive lens," *Opt. Exp*. **14**, 3847-3852 (2006) [doi:10.1364/OE.14.003847].
[25] X. Chen and S. R. J Brueck, "Imaging interferometric lithography: approaching the resolution limits of optics," *Opt. Lett*. **24**, 124-126 (1999) [doi:10.1364/OL.24.000124].
[26] V. Mico, Z. Zalevsky, and J. García, "Superresolution optical system by common-path interferometry," *Opt. Exp*. **14**, 5168-5177 (2006) [doi:10.1364/OE.14.005168].
[27] V. Mico, Z. Zalevsky, and J. García, "Common-path phase-shifting digital holographic microscopy: a way to quantitative imaging and superresolution," *Opt. Comm*. **281**, 4273–4281 (2008) [doi:10.1016/j.optcom.2008.04.079].